



# Extraction of weak fault transients using variational mode decomposition for fault diagnosis of gearbox under varying speed

Vikas Sharma<sup>a,\*</sup>, Anand Parey<sup>b</sup>

<sup>a</sup> Department of Mechanical and Aerospace Engineering, Seoul National University, Seoul 08826, Republic of Korea

<sup>b</sup> Discipline of Mechanical Engineering, Indian Institute of Technology Indore, India



## ARTICLE INFO

### Keywords:

Fault diagnosis  
Demodulation  
Vibration signal  
Gearbox  
Varying speed

## ABSTRACT

Non-stationary vibration signals of a gearbox under varying speed display complicated modulations, which lead to intense sidebands thereby resulting in difficulty to identify the presence of a fault. Variational mode decomposition (VMD) being highly adaptive, effective in attenuating mode-mixing problem, low computational time requirement and therefore it is suitable to decompose a modulated multi-component non-stationary gearbox vibration signal. This research work thus utilizes the merits of VMD for demodulation and to diagnose localized gear tooth faults under real-time speed variation. In the present study, the vibration signals of a gearbox for different faults were acquired under complete speed variation (i.e., run-up, random fluctuation, and coast-down). To identify the symptoms confirming the presence of faults, the vibration signals were decomposed by VMD thereby demodulating the raw vibration signal. The decomposed VMFs exhibited the presence of transients due to faults and were analyzed statistically. To state the effectiveness of VMD in exhibiting fault by extracting fault transients, the performance of VMD was compared with the performance of recently developed wavelet based empirical wavelet transform (EWT) and flexible analytic wavelet transform (FAWT). The fault detection performance of VMD outperforms EWT as demonstrated by simulated signal and validated by the experimental investigations. FAWT was found ineffective in decomposing the vibration signal under varying speed.

## 1. Introduction

Gearboxes are crucial machine assemblies of wind turbines, employed to transmit torque thereby assisting in renewable power generation. In wind turbines, gearboxes are bound to operate under varying speed due to the changing wind direction and non-constant velocity [1–5] as shown in Fig. 1. Varying speed makes a gearbox prone to failure even before the designed life of a gearbox. Therefore, it becomes highly necessary to monitor the health of a gearbox and thereby detecting the occurrence of any possible failure. Vibration-based health-monitoring mechanisms are important elements of a health monitoring system and have proved their effectiveness in early fault diagnosis [6]. For more than two and a half decades, a huge amount of research on various vibration-based fault diagnosis approaches has been reported inclusive of dynamic modeling based simulations and signal processing based experimental analysis under constant and varying operating conditions [6–11].

Vibration signals of a gearbox are influenced by friction, time-varying mesh stiffness, tooth profile uncertainties and non-stationary operating conditions [11]. The weak fault transients generated by the meshing of incipient fault present in a tooth of gear is

\* Corresponding author.

E-mail address: [s.vikasiiti@gmail.com](mailto:s.vikasiiti@gmail.com) (V. Sharma).

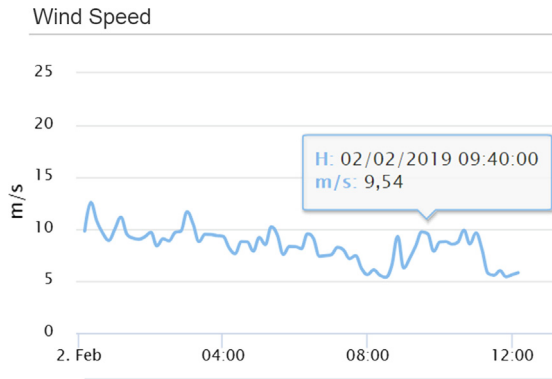


**Fig. 1.** A screenshot of real-time wind speed recorded for operating Wind Turbine on 02/02/19 [4].

also trapped by strong background noise. In real-time conditions, fluctuations occurring in the speed of a gearbox results in the smearing of frequencies in frequency spectrums. Consequently, it becomes difficult to separate the useful information from the noisy signal i.e. unable to locate the characteristic fault frequencies. Thus, at varying speed conditions, conventional techniques such as fast Fourier transform (FFT), time-synchronous averaging (TSA), cepstrum, entropy analysis, etc. turns ineffective for fault diagnosis of gearboxes [6–8]. Methods based on spectral analysis alone [12,13] were observed incompetent, as they also produce erroneous results; further, they are limited to non-stationary speed and load conditions. Despite the crucial achievements by the conventional methods, each of these methods has their own limitation towards condition monitoring and early fault diagnosis at varying speed conditions.

Non-stationary signal processing techniques such as wavelet transform (WT) [12], empirical mode decomposition (EMD) [13] and variational mode decomposition (VMD) [14] are suitable for condition monitoring of mechanical systems. WT decomposes signals using filter bands, thereby restricting to have mono frequency components. WT is also constrained by the Heisenberg uncertainty principle [12], which explains that perfect time and frequency localization cannot occur simultaneously. Additionally, WT suffers from issues related to the mother-wavelet-selection criteria, border distortion, energy leakage [15,16]. On the contrary, both EMD and VMD are specialized in decomposition without any predefined basis. They decompose a signal into  $n$  band components. A serious problem in the application of EMD is boundary distortion of IMFs; while performing statistical analysis of IMFs, boundary distortion may provide high values of CIs, even if a fault is absent [17]. EMD being an adaptive method, despite mode mixing, sensitivity to noise and sampling limits its performance, as well as EMD, lacks mathematical description [18]. Researchers such as Parey and Pachori [19], Sharma and Parey [20], Deng et al. [21] and Zhong and Shixiong [22] have tried to solve the problems of EMD. Methods such as ensemble empirical mode decomposition [23], synchrosqueezing [24,25], empirical wavelets [26] were partially successful in addressing the EMD problems.

Most of these researches evaluated the fault diagnosis methods under either constant speed or particular specific speed conditions, and rely on the assumption of hypothetical data, computational complexity, and signal stationarity. Nevertheless, in real-world circumstances, gearboxes often operate under time-varying conditions, and their vibration signals are multi-component, modulated and non-stationary. To the best of our knowledge, the research and investigations on a gearbox under varying speed are very limited in the continuous growing literature. The main contribution of this work is outlined as follows:

- (1) A novel proposed technique – variational mode decomposition – is first applied for demodulation of modulated non-stationary vibration signals and adaptive signal decomposition thereby exhibiting and detecting fault transients caused by gear-meshing of faulty gears;
- (2) The speed variation performed to examine the performance of the VMD resembles the real-time speed variation (i.e., run-up, random fluctuation, and coast-down) as shown in Fig. 1, not yet studied before [4,5,15,20,26–33];
- (3) The comparisons are thoroughly conducted demonstrating a numerically simulated signal and a practical vibration signal, in order to investigate the effectiveness of the proposed method with recently developed wavelet-based decomposition methods viz. empirical wavelet transform (EWT) and flexible analytic wavelet transform (FAWT). These have also been used for gear fault diagnosis under non-stationary conditions.

The remaining structure of the manuscript is organized as follows. VMD algorithm and equivalent filter banks of EWT and FAWT along with their characteristics are reviewed in Section 2. In Section 3, VMD is applied to detect faulty transients of a simulated gear vibration signal and FFTs are plotted for the VMFs to exhibit the frequency components. A comparison of VMD, EWT, and FAWT for a simulated signal is presented subsequently. Section 4, demonstrates VMD based extraction of faulty transients for experimentally acquired vibration signals under real-time speed variation followed by the comparison of VMD with other methods. The conclusion is reported in Section 5.

## 2. Proposed method for gear fault diagnosis

### 2.1. Variational mode decomposition (VMD) method

VMD [14] decomposes a real-valued signal  $r(t)$  into  $K$  narrow-band components  $s_k(t)$ . It also computes the center frequencies  $\omega_k$  where  $k = 1, 2, \dots, K$ . In order to obtain these narrow-band components and their corresponding center frequencies, this method formulates constrained optimization problem [34]. Before the formulation of the optimization problem, the Hilbert transform is applied to the components  $s_k(t)$  in order to compute the unilateral frequency spectrum. After that, modulation property is used to shift the frequency spectrum of these components based on the estimated center frequencies  $\omega_k$ . The bandwidth was estimated through the H Gaussian smoothness of the demodulated signal [14]. Now, the constrained optimization problem is formulated as [14]:

$$\min_{\{s_k\}, \{\omega_k\}} \left\{ \sum_k \left\| \partial_t \left[ \left( \delta(t) + \frac{j}{\pi t} \right) * s_k(t) \right] e^{-j\omega_k t} \right\|_2^2 \right\} \quad (1)$$

such that  $\sum_k s_k(t) = r(t)$  and  $*$  denotes the convolution,  $\|\cdot\|_2^2$  represents the squared  $L^2$  norm,  $\delta$  is the Dirac delta distribution. The Lagrangian multiplier ( $\lambda$ ) has been applied to convert the constrained optimization problem (Eq. (2)) into an unconstrained optimization problem. The unconstrained optimization problem can be expressed as [14]:

$$L(\{s_k\}, \{\omega_k\}, \lambda) := \alpha \sum_k \left\| \partial_t \left[ \left( \delta(t) + \frac{j}{\pi t} \right) * s_k(t) \right] e^{-j\omega_k t} \right\|_2^2 + \|r(t) - \sum_k s_k(t)\|_2^2 + \langle \lambda(t), r(t) - \sum_k s_k(t) \rangle \quad (2)$$

In Eq. (2), parameter  $\alpha$  is the penalty factor. The estimated narrow-band component and corresponding center frequency during  $n + 1$  iteration can be computed as follows [14]:

$$\hat{s}_k^{n+1}(\omega) = \frac{\hat{r}(\omega) - \sum_{i \neq k} \hat{s}_i(\omega) + \frac{\hat{\lambda}(\omega)}{2}}{1 + 2\alpha(\omega - \omega_k)^2} \quad (3)$$

$$\omega_k^{n+1} = \frac{\int_0^\infty \omega |\hat{s}_k(\omega)|^2 d\omega}{\int_0^\infty |\hat{s}_k(\omega)|^2 d\omega} \quad (4)$$

In Eqs. (4) and (5),  $\hat{r}(\omega)$ ,  $\hat{s}_k(\omega)$ ,  $\hat{s}_k^{n+1}(\omega)$  and  $\hat{\lambda}(\omega)$  represent the Fourier transform of  $r(t)$ ,  $s_k(t)$ ,  $s_k^{n+1}(t)$  and  $\lambda(t)$  respectively. The update in  $\lambda$  can be expressed by following expression [35]:

$$\hat{\lambda}^{n+1}(\omega) = \hat{\lambda}^n(\omega) + \tau \left[ r(\omega) - \sum_k \hat{s}_k^{n+1}(\omega) \right] \quad (5)$$

where  $n$  is the number of iterations. More details about the methods can be found in Ref. [14].

In VMD method, the tolerance of convergence ( $tol$ ) parameter is useful for controlling the relative errors corresponding to the estimated narrow-band components. Interestingly, the expression of  $\hat{s}_k^{n+1}(\omega)$  in Eq. (4) contains a wiener filter structure for denoising [14]. The  $\hat{s}_k^{n+1}[n]$  can be computed from the real part of the inverse Fourier transform applied on  $\hat{s}_k^{n+1}(\omega)$ . The advantages of VMD technique are as follows:

- (1) The relative error is largely independent of the harmonic's frequency and is controlled by tolerance level.
- (2) The VMD achieves good tones separation [36].

### 2.2. Filter banks and characteristics of FAWT

FAWT is similar to WT with constant Q-factor (the ratio of the center frequency to the bandwidth) but improvises the decomposition by additional high-pass filters. FAWT consists of one low-pass and two high-pass filters. One of these high-pass filters analyzes 'positive frequencies', while the other analyzes 'negative frequencies'. The filters are expressed as:

$$H(\omega) = \begin{cases} \sqrt{pq}, & |\omega| \leq \omega_p \\ \sqrt{pq}\theta[(\omega - \omega_p)/(\omega_s - \omega_p)], & \omega_p \leq |\omega| \leq \omega_s \\ \sqrt{pq}\theta[(\pi - \omega + \omega_p)/(\omega_s - \omega_p)], & -\omega_s \leq |\omega| \leq -\omega_p \\ 0, & |\omega| \geq \omega_s \end{cases} \quad (6)$$

$$G(\omega) = \begin{cases} \sqrt{2rs}\theta[(\pi - \omega + \omega_0)/(\omega_1 - \omega_0)], & \omega_0 \leq |\omega| \leq \omega_1 \\ \sqrt{2rs}, & \omega_1 \leq |\omega| \leq \omega_2 \\ \sqrt{2rs}\theta[(\omega - \omega_2)/(\omega_3 - \omega_2)], & \omega_2 \leq |\omega| \leq \omega_3 \\ 0, & \omega \in [(0, \omega_0) \cup (\omega_3, 2\pi)] \end{cases} \quad (7)$$

where  $H(\omega)$  is the frequency response of the scaling function; whereas,  $G(\omega)$  make up the frequency response of analytic wavelet function.  $\beta$  and  $\varepsilon$  are the non-negative constants and must satisfy  $\beta < 1$ , then

$$\omega_p = \frac{1 - \beta}{p}\pi + \frac{\varepsilon}{p}, \quad \omega_s = \frac{\pi}{p}, \quad \varepsilon = \frac{1}{32} \left( \frac{p - q + \beta q}{p + q} \right) \pi$$

$$\theta(\omega) = \frac{1}{2}(1 + \cos\omega)\sqrt{2 - \cos\omega} \quad \forall \quad \omega \in [0, \pi]$$

$$\omega_0 = \frac{1 - \beta}{r}\pi + \frac{\varepsilon}{r}, \quad \omega_1 = \frac{p\pi}{qr}, \quad \omega_2 = \frac{\pi - \varepsilon}{r}\omega_3 = \frac{\pi + \varepsilon}{r}$$

It reveals that  $\beta$  determines the quality factor of FAWT. The range of  $\beta$  is determined as  $\beta \in [1 - p/q, 1]$ . The small values of  $\beta$  will lead to fine-frequency resolution of FAWT. A detailed description of FAWT can be read from a paper by Bayram [37].

### 2.3. Filter banks of EWT

To introduce the adaptive features in wavelets, EWT was proposed by Gilles [38] to improvise its performance in signal decomposition. The fundamental idea is to segment the Fourier spectrum of amplitude modulation (AM) - frequency modulation (FM) signal followed by applying some filtering. The empirical scaling function and empirical wavelets are expressed by the following expressions [38]:

$$\phi_n(\omega) = \begin{cases} 1, & |\omega| \leq (1 - \gamma)\omega_n \\ \cos \left[ \frac{\pi}{2} \beta \left( \frac{1}{2\gamma\omega_n} (|\omega| - (1 - \gamma)\omega_n) \right) \right], & (1 - \gamma)\omega_n \leq |\omega| \leq (1 + \gamma)\omega_n \\ 0, & \text{otherwise} \end{cases} \quad (8)$$

$$\psi_n(\omega) = \begin{cases} 1, & (1 + \gamma)\omega_n \leq |\omega| \leq (1 - \gamma)\omega_{n+1} \\ \cos \left[ \frac{\pi}{2} \beta \left( \frac{1}{2\gamma\omega_{n+1}} (|\omega| - (1 - \gamma)\omega_{n+1}) \right) \right], & (1 - \gamma)\omega_{n+1} \leq |\omega| \leq (1 + \gamma)\omega_{n+1} \\ \sin \left[ \frac{\pi}{2} \beta \left( \frac{1}{2\gamma\omega_n} (|\omega| - (1 - \gamma)\omega_n) \right) \right], & (1 - \gamma)\omega_n \leq |\omega| \leq (1 + \gamma)\omega_n \\ 0, & \text{otherwise} \end{cases} \quad (9)$$

To ensure that the set consisting of the empirical scaling function and all empirical wavelets is a tight frame of  $L^2(R)$  the function  $\beta(\omega)$  and  $\gamma$  must satisfy:

$$\beta(\omega) = \omega^4(35 - 84\omega + 70\omega^2 - 20\omega^3) \quad \text{and} \quad \gamma = \min_n \left( \frac{\omega_{n+1} - \omega_n}{\omega_{n+1} + \omega_n} \right)$$

Further, both approximated coefficients and detailed coefficients are derived by the inner products as per the traditional wavelet theory as [38]:

$$W_f^\varepsilon(0, t) = \langle f, \phi_1 \rangle = \int f(\tau) \phi_1(\tau - t) d\tau \quad (10)$$

$$W_f^\varepsilon(n, t) = \langle f, \psi_n \rangle = \int f(\tau) \psi_n(\tau - t) d\tau \quad (11)$$

Then the empirical modes are extracted as [38]:

$$f_0(t) = W_f^\varepsilon(0, t) * \phi_1(t) \quad (12)$$

$$f_k(t) = W_f^\varepsilon(k, t) * \psi_k(t) \quad (13)$$

For detail description of the method can be found in a paper by Gilles [38].

### 2.4. Condition indicators (CIs)

Condition indicators (CIs) are used to quantify the level (in order to notice an incipient fault that may be of low severity) of vibrations generated due to appearing fault phenomenon. A brief description of the CIs used in this study is expressed as follows:

- (1) Root mean square (R.M.S) – It is defined as the square root of the mean of the sum of the squares of sample signals. It reflects a vibration amplitude and energy of a signal in the time domain [10].

$$RMS = \sqrt{\frac{1}{N} \sum_{i=1}^N (x_i)^2} \quad (14)$$

- (2) Kurtosis – It is used to reflect the presence of impulses in a signal. It is fourth-order normalized moment of a given signal and is

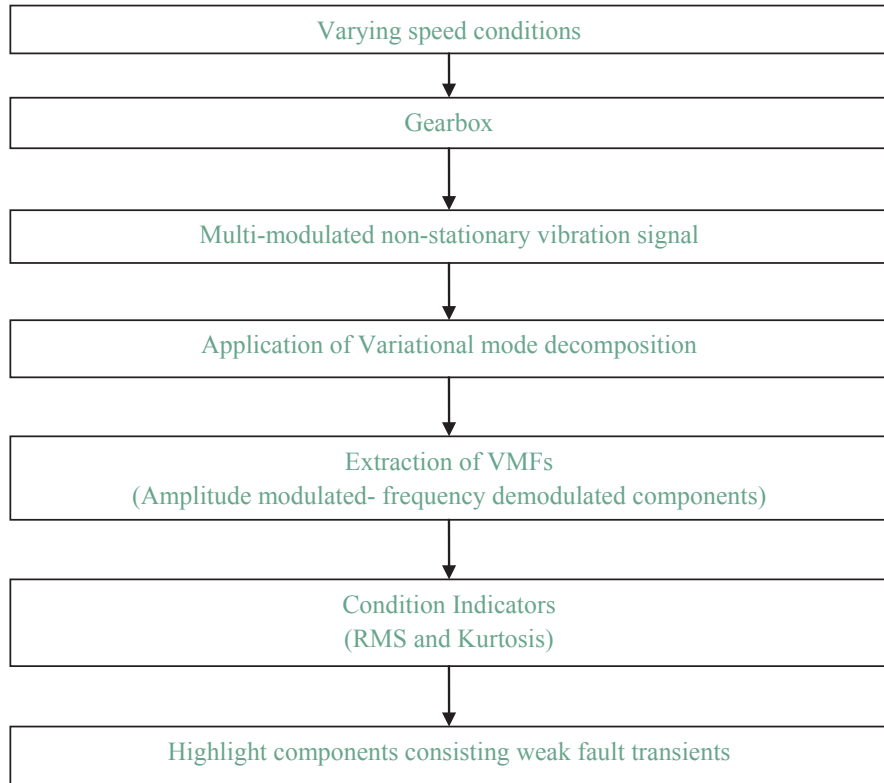


**Fig. 2.** Overall procedure of the method.

expressed as [10]:

$$k = \frac{N \sum_{i=1}^N (x_i - \bar{x})^4}{\left( \sum_{i=1}^N (x_i - \bar{x})^2 \right)^2} \quad (15)$$

where,  $x$  is the original sample,  $i$  is the number of samples and  $\bar{x}$  is the mean. A signal consisting exclusively of Gaussian distributed data will have a kurtosis of approximately 3 [39,40]. The increase in the kurtosis value highlights peakedness present in the distribution of the signal.

A very basic procedure is adopted for the extraction of weak fault transients from a gearbox vibration signal under varying speed to detect the gear faults. The objective of the manuscript is to emphasize the demodulation capability of the VMD in extracting transients. Research discussing such a comparative investigation of VMD to FAWT and EWT has not been reported yet under varying speed conditions. Therefore, decomposition performance of VMD is compared to its contemporary signal decomposition techniques such as FAWT or EWT additionally. The flowchart of the overall procedure is reported in Fig. 2.

VMD is an adaptive technique based on the combination of Hilbert transform, wiener filter and norm which has an advantage of solving the mode-mixing error of the classical EMD and eliminating unwanted noise components. Mode-mixing occurs because of variation in phase of the signal components at different time instants resulted by varying speed conditions. When VMD is applied to a signal its Hilbert transform is calculated followed by the analytical signal of a unilateral frequency spectrum. Upon solving convolution i.e., modulation property is used to shift the frequency spectrum based on the estimated center frequencies and bandwidth. Thus, frequency demodulated signal components are extracted concurrently in a non-recursive manner.

### 3. Simulation of a gear fault under varying speed

A simulation study was conducted on a simple yet realistic gear synthetic signal, which consisted of both AM-FM signal [20–23] along with a periodic double-sided asymmetric transient to illustrate the effectiveness of fault diagnosing capability of the proposed approach.

### 3.1. Vibration signal model of a locally damaged fixed axis gearbox

A mathematical model for expressing gear vibrations with a localized fault in one of the gears along with exhibiting the characteristics of the gearbox in operation, a synthetic signal  $x(t)$  containing additive random noise  $\text{noise}(t)$  can be written as:

$$x(t) = x_1(t) + x_2(t) + \text{noise}(t) \quad (16)$$

$$x_1(t) = \sum_{m=0}^M X_m [1 + a_m(t)] \cos[2\pi m Z f_r t + \Phi_m + b_m(t)] \quad (17)$$

where  $x_1(t)$  is the AM-FM harmonic signal,  $f_r$  is the gear rotating frequency and  $Z$  is the number of teeth on the gear. Therefore, gear mesh frequency (GMF) can be calculated by  $Z f_r$ ,  $m$  is the number associated with harmonic of GMF,  $X_m$  is the amplitude of  $m^{\text{th}}$  harmonics of GMF,  $\Phi_m$  is the original phase,  $a_m(t)$  and  $b_m(t)$  are the AM functions.

$$\text{where, } a_m(t) = \sum_{m=1}^{M_s} A_{mn} \cos(2\pi f_r t + \alpha_{mn}) \quad \text{and} \quad b_m(t) = \sum_{m=1}^{M_s} B_{mn} \cos(2\pi f_r t + \beta_{mn}) \quad (18)$$

$A_{mn}$  and  $B_{mn}$  are the amplitudes  $\alpha_{mn}$  and  $\beta_{mn}$  are the phases of  $n^{\text{th}}$  sidebands of the amplitude around  $m^{\text{th}}$  meshing harmonic. Bonnardot et al. [4] suggested that  $f_r$  could be substituted by  $f_r(i)$  under the condition of varying speed, therefore, Eq. (17) can be rewritten as follows:

$$x_1(t) = \sum_{m=0}^M X_m [1 + a_m(t)] \cos[2\pi m Z f_r(i) t + \Phi_m + b_m(t)] \quad (19)$$

Another component  $x_2(t)$  that represents the localized tooth fault phenomenon can be modeled as a double-side asymmetric transient as follows:

$$x_2(t) = \sum_k h(t - T_0 - kT) \quad (20)$$

where  $h(t)$  is single transient and keeping time index  $T_0$  as 0.05 s and time period  $T$  as 0.1 s for time center ( $kT + T_0$ ) of  $k^{\text{th}}$  transient. To perform simulation for a single harmonic of gear, the values of  $m = 1$ ,  $M_s = 1$  were considered. The values of  $T_0$  and  $T$  depend on the rotational speed of gears and are part of transient impulse. For the present simulation case, this transient impulse that will appear for less than a second, more precisely for 0.1 s as the gear was considered running at 10 Hz and one impulse will appear for one revolution. Therefore, the values of  $T_0$  and  $T$  were taken as 0.05 and 0.1 respectively. Now, this  $h(t)$  is expressed as follows:

$$h(t) = \begin{cases} e^{-\sigma_f/\sqrt{1-\sigma_f^2}} (2\pi f_0 t)^2 \cos(2\pi f_0 t), & t \leq 0 \\ e^{-\sigma_f/\sqrt{1-\sigma_f^2}} (2\pi f_0 t)^2 \cos(2\pi f_0 t), & t > 0 \end{cases} \quad (21)$$

where  $f_0$  is the fault frequency generated due to the impulse of localized fault. For different meshing frequencies, there will be different fault frequencies. For simulation, the value of  $f_0$  is assumed as 220 Hz with left and right damping ratio be 0.02 and 0.01 respectively. For simulation, run-up conditions were considered therefore, the input frequency of shaft was assumed to run from 10 Hz to 15 Hz as shown in Fig. 3; the number of teeth on gear was taken as 32. The sampling frequency kept for the simulation was 4.096 kHz. The values of other variables for simulation purpose were assumed as  $X_m = 5$ ,  $A_{mn} = B_{mn} = 0.05$ ,  $\alpha_{mn} = \beta_{mn} = 0$ . The signals developed from these equations have been displayed in Fig. 4. In Fig. 4(a), a pure AM-FM signal was observed under varying speed conditions. Fig. 4(b) shows the time response impulses generated due to a localized fault. Fig. 4(c) shows the complete signal  $x(t)$  inclusive of random noise of surrounding, as given in Eq. (16). While performing simulation, the noise was kept high intentionally to mask the fault components presents in the signals and to evaluate the proposed approach. Fig. 5 shows the FFT of the simulated signal at varying speed conditions. From Fig. 5(b), it was difficult to highlight the GMF due to smearing of the frequencies. Further, impacts developed by the transients cannot be directly detected either in the time domain or in the frequency domain (Fig. 5). Table 1 gives an idea about the performance of condition indicators RMS and kurtosis. It was observed that after inducing the fault transients as mentioned in Eqs. (20) and (21), the kurtosis and RMS were unable to differentiate the different states of the

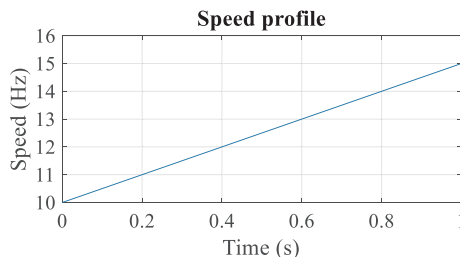
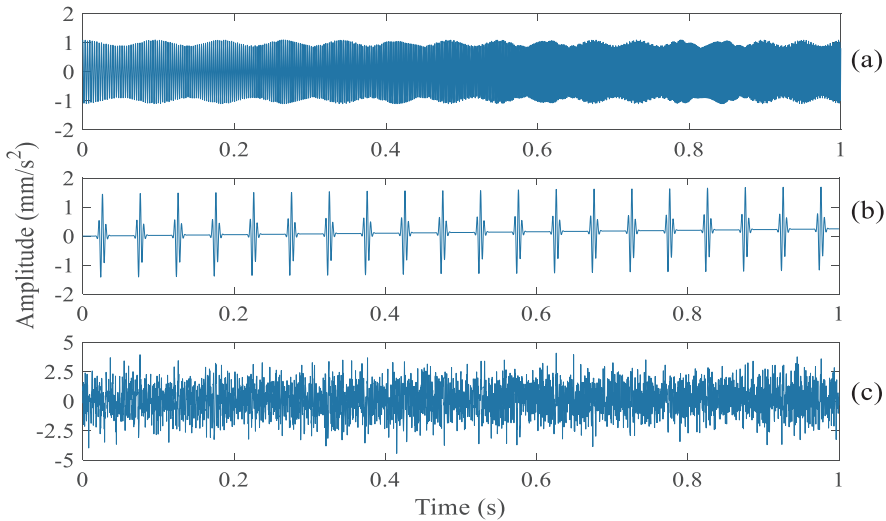
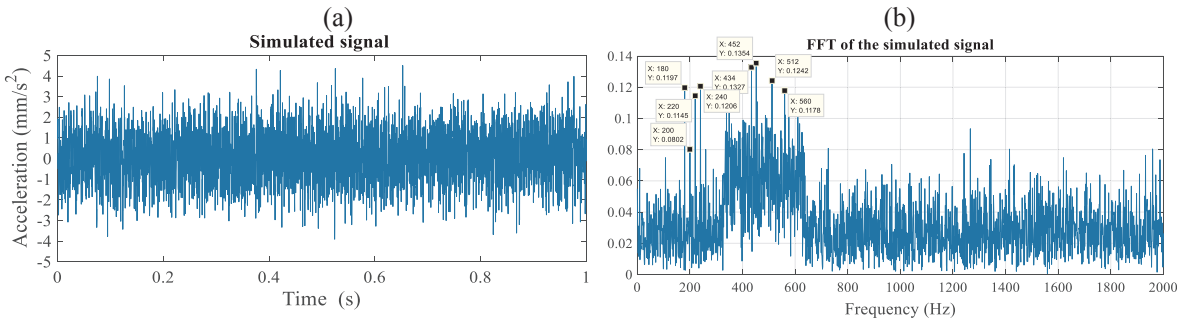


Fig. 3. Linearly increasing speed profile for the simulation study.



**Fig. 4.** Simulated signals; (a) AM-FM signal, (b) fault transients, (c) combined signal with noise.



**Fig. 5.** (a) Simulated signal; (b) FFT of the signal.

**Table 1**  
Performance of CIs for raw simulated vibration signals under varying speed.

Signal	Condition indicators	
	RMS	Kurtosis
No fault	1.2328	2.8254
With fault	1.2807	2.8410

simulated vibration signals under varying speed conditions. Therefore, advanced non-stationary signal processing was required for effective fault detection by exhibiting the faulty transients masked under heavy noise.

### 3.2. Demonstration of simulation results and performance evaluation

A simulation study was performed by generating a gear vibration signal at run-up conditions from the simulation model of fixed axes gearbox. The objective of this research is to reveal the presence of fault transients generated due to the meshing of the faulty tooth trapped in the heavy noise of a gear vibration signal. Fundamentally, if there is any localized gear tooth fault, then either an increase in the amplitude of sidebands or an increase in the number of sidebands around the GMF is observed [41–43]. Fig. 6 shows the VMFs and their respective FFTs are presented to state the different frequency components present in the simulated signal. To gain more insights about the frequency components enlarged view of two VMFs and their respective FFTs are presented in Fig. 7. VMF<sub>1</sub> presented in Figs. 6 and 7(a) clearly depicts the occurrence of faulty transients. These transients are occurring at the regular interval as visible from the reading of markers. The FFTs of the VMFs display that VMFs are capable to decompose the simulated vibration signal under varying speed conditions. It is clearly observed from Fig. 6 that the VMF<sub>1</sub> corresponds to faulty transient whereas; VMF<sub>2</sub>, VMF<sub>3</sub>, and VMF<sub>4</sub> show the decomposition of simulated signals at varying speed. The VMF<sub>3</sub> component presented in Fig. 7(c) depicts the presence of 500 Hz frequency components that could possibly be GMF as 500/32 gives 15.6 Hz that can be related as the

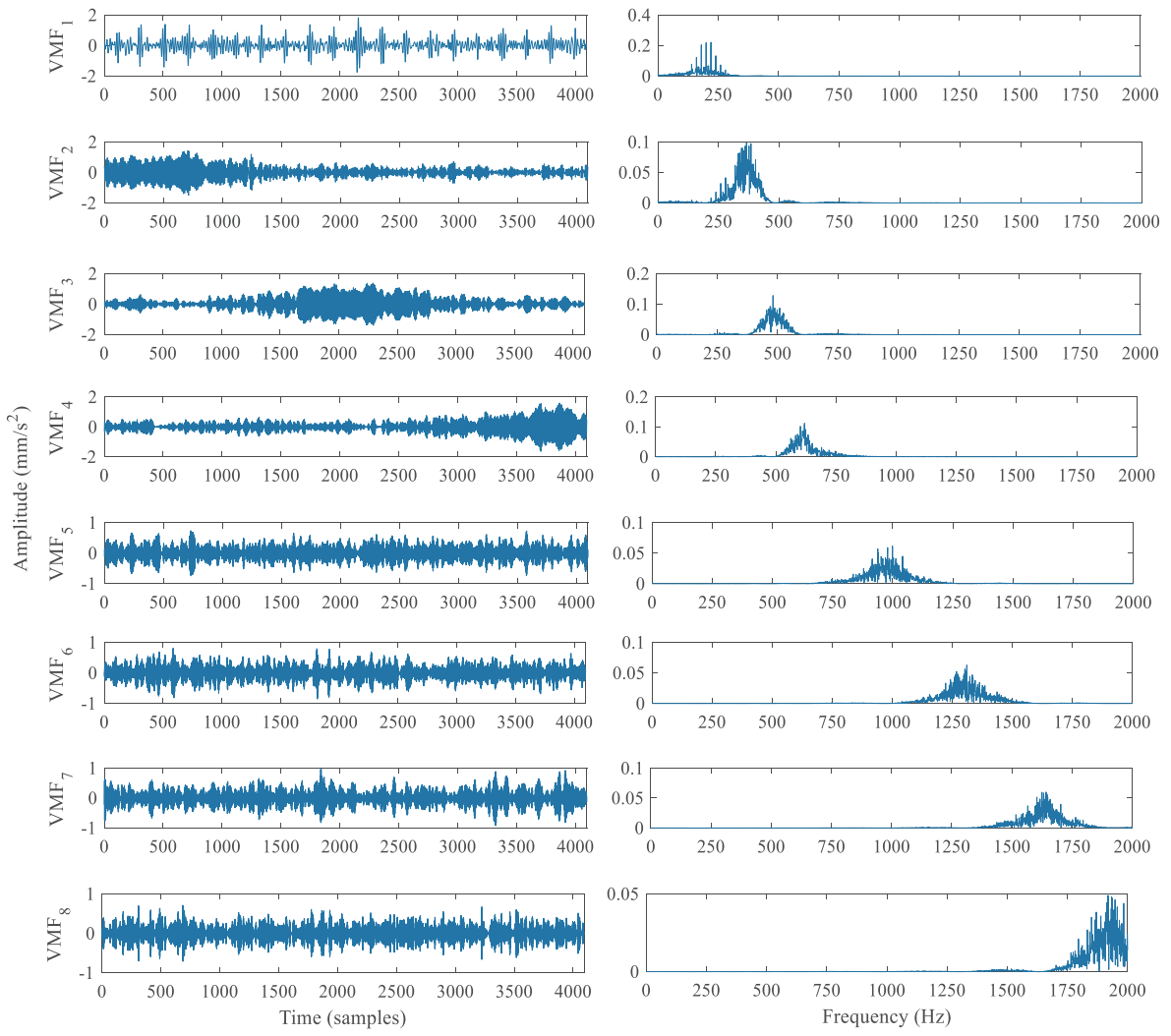


**Fig. 6.** Decomposition by VMD into VMFs and their FFTs.

maximum input speed given in the simulation.

The FFT of the subsequent mode function i.e., VMF<sub>3</sub> onwards reflects higher frequency signal components, which may resemble noise or unwanted signal components. Further analysis of the decomposed VMFs of the simulated vibration signal for both no-fault and with-fault, the CIs were evaluated and reported in Table 2. It can be referred from Table 2, that the initial few decomposed mode functions have reflected as gain in the kurtosis that highlights the presence of a fault. Moreover, for a few initial mode functions RMS also increases for faulty gear simulated signal. To analyze the speed of decomposition of VMD, the computation time for solving the entire simulation was calculated. Simulations were performed using Matlab2016b on Intel (R) Core (TM) i7-7700 CPU @ 3.60 GHz with installed memory of 16 GB on a 64-bit Operating System.

Further, the same simulated signal was decomposed using EWT to analyze the present frequency components. It decomposed the varying simulated speed into different modes to compensate for the speed variation. Fig. 8 highlights the decomposed components presented as mode functions (MFs) and their respective FFTs. From Fig. 8, it was observed that EWT decomposes a signal in narrow-band spectrums with respect to the variation in the signal components; therefore, more levels of decompositions were required for the entire signal. However, to compare the performance of EWT versus VMD as well as to expose the frequency components via decomposed components only a few decomposed components are shown. Fig. 9 shows the enlarged view of the FFTs of the decomposed components. In Fig. 8, the transient faults are not clearly visible; however, the vibrations based on speed variation can be seen decomposed from MF5 to MF9. From Fig. 9, it was observed that the frequency components present in the FFTs of the decomposed MF were not completely separated. Table 3, presents the statistical analysis of the MF obtained from EWT. The RMS and kurtosis were not been found sensitive with respect to the presence of faults. Moreover, the computation time of the EWT was also observed increasing. Thus, it can be reported that EWT gives mixed output in terms of decomposition such as frequency components are visible but not in the specific frequency band, presence of fault transients is not clear from the decomposed MFs. Nevertheless, the statistical indicators show the increased response for two MFs with the presence of a fault. There is a further need to revise the algorithm of

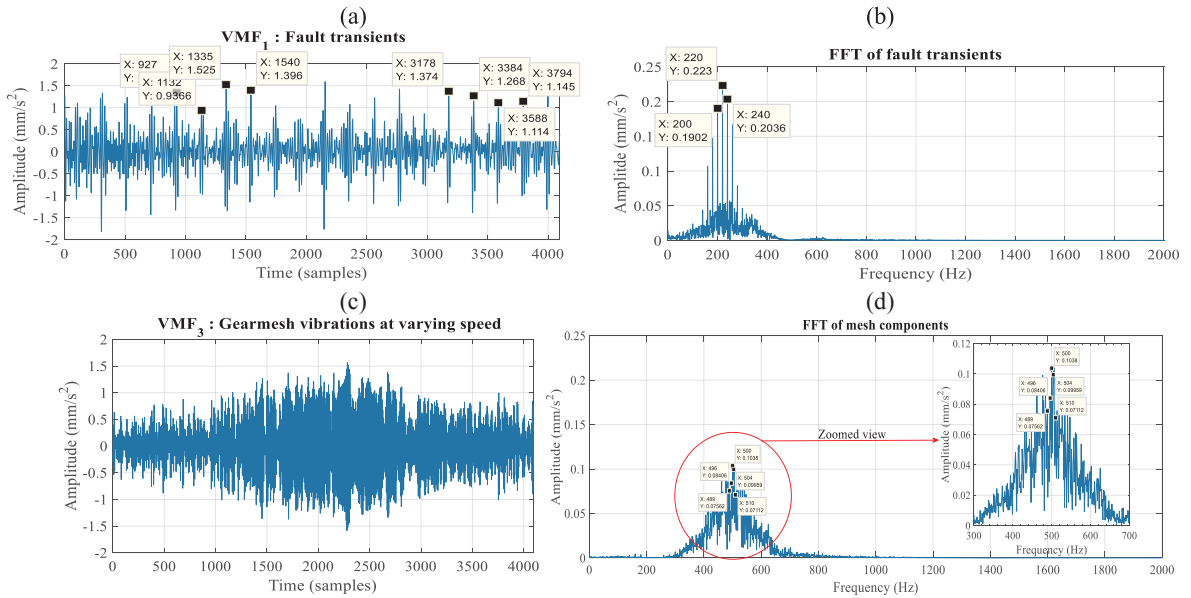


**Fig. 7.** Detailed view of decomposed VMFs: VMF<sub>1</sub> and its FFT ((a) and (b)), VMF<sub>3</sub> and its FFT ((c) and (d)).

**Table 2**  
Performance of CIs post-VMD.

Signal Decomposed mode	No fault Condition Indicator		With fault Condition Indicator	
	RMS	Kurtosis	RMS	Kurtosis
VMF <sub>1</sub>	0.2381	<b>3.0544</b>	0.3690	<b>4.6568</b>
VMF <sub>2</sub>	0.2847	<b>3.5956</b>	0.3822	<b>4.1647</b>
VMF <sub>3</sub>	0.3199	<b>3.9790</b>	0.4181	<b>5.9888</b>
VMF <sub>4</sub>	0.3915	4.3075	0.3907	4.3208
VMF <sub>5</sub>	0.2369	2.9465	0.2367	2.9470
VMF <sub>6</sub>	0.2512	2.7531	0.2511	2.7531
VMF <sub>7</sub>	0.2318	3.0609	0.2317	3.0616
VMF <sub>8</sub>	0.2423	2.8413	0.2423	2.8417
Processing Time (s)	3.7050		3.4542	

EWT for effective decomposition and sparse representation of faulty transients.

Decomposition by FAWT into MFs and their respective FFTs are plotted in Fig. 10. Eight MFs were obtained from the FAWT to decompose the entire signal. The statistical analysis of the obtained MF using condition indicators RMS and kurtosis were evaluated and reported in Table 4. The enlarged view of the first MF depicting the low-frequency signal components by FAWT is shown in Fig. 11.

FAWT failed to decompose the signal into different significant and crucial frequency components. The low-frequency MF is very much similar to the FFT of the original simulated vibration signal. The MF<sub>1</sub> does not clearly exhibit the GMF and the fault frequencies embedded in the simulated signal mentioned in Eq. (21). Neither the faulty transients were extracted by FAWT nor did the condition indicators sense the presence of faults present in the decomposed MFs under varying speed conditions. Further, the time consumption by FAWT was found twice than that of VMD and the decomposition was not impressive i.e., frequency components were not separated.

This concludes the simulation study on extraction of faulty transients for gear fault diagnosis under varying speed conditions and it was observed that FAWT is incapable of decomposing a vibration signal. The best decomposition was recorded by VMD followed by EWT. Further, the performance of condition indicators was also found better with VMD. The experimental investigations to explore the faulty transients present in the vibration signal acquired under real-time varying speed conditions have been performed in the next section of the manuscript.

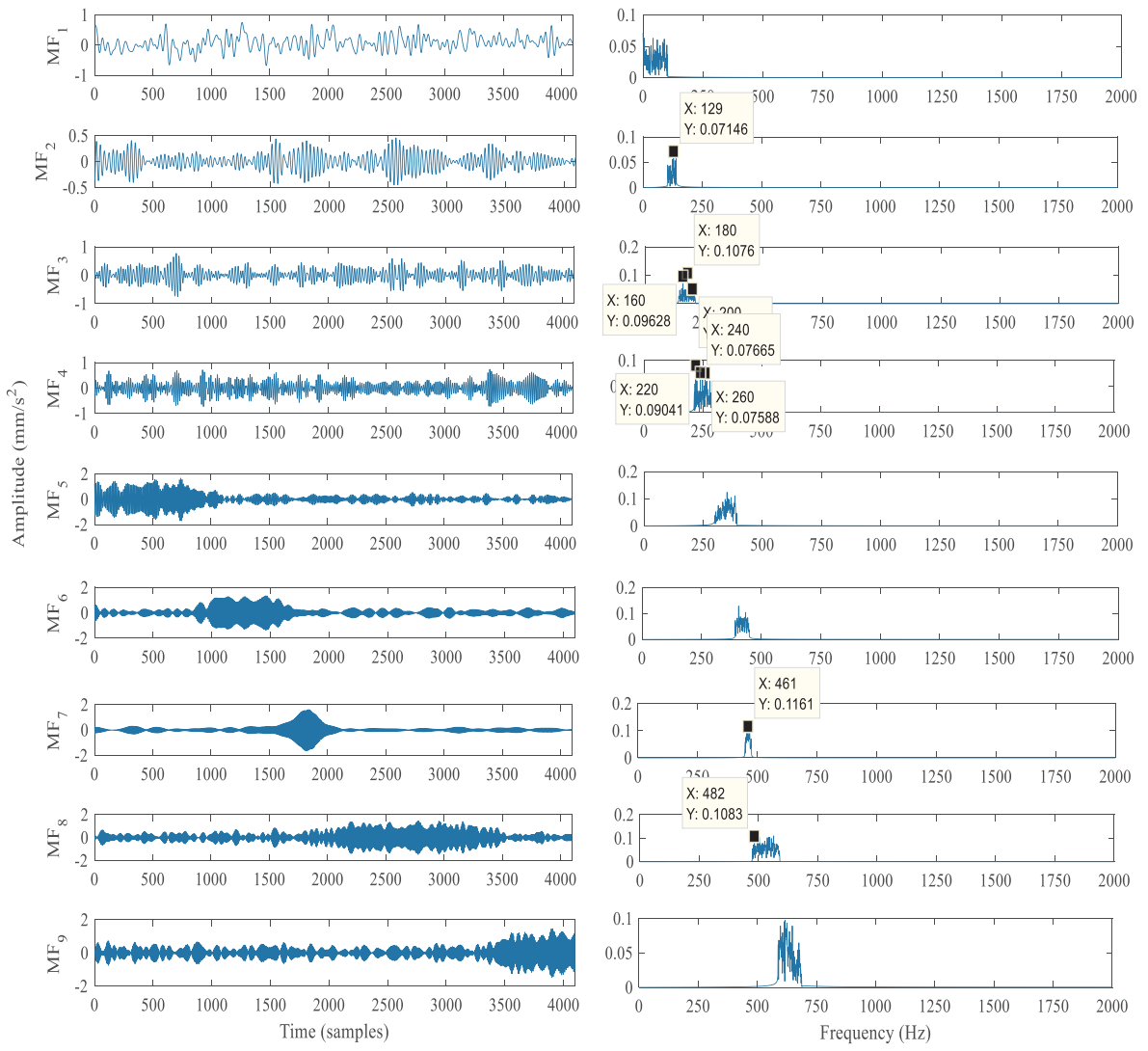


**Fig. 8.** Decomposition by EWT into mode functions (MFs) and their FFTs.

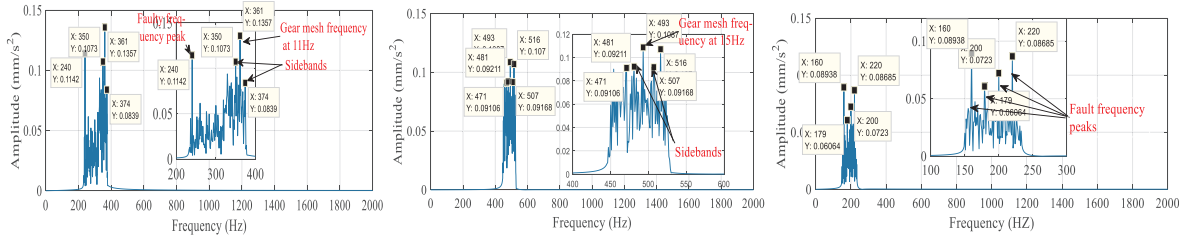


**Fig. 9.** Detailed view of FFTs of different mode functions (from Fig. 8).

#### 4. Experimental evaluation

##### 4.1. Test rig

To investigate the presence of fault transients in the gear vibration signal using VMD, experiments were carried out on a simple motor-drive-brake type gear test rig (Drivetrain Diagnostic Simulator) as shown in Fig. 12(a). It consists of an AC motor (3 phase, 2.237 kW) to drive the test rig. This motor can be operated up to a speed of 3000 rpm with a continuous variation using motor control module of NV Gate. A magnetic brake type loading arrangement was used to apply a maximum radial load of 88 Nm (at the test gear)

**Table 3**  
Performance of CIs post EWT.

Signal Decomposed mode	No fault Condition Indicator		With fault Condition Indicator	
	RMS	Kurtosis	RMS	Kurtosis
MF <sub>1</sub>	0.1765	3.7383	0.1889	3.6526
MF <sub>2</sub>	0.1916	<b>2.5765</b>	0.1972	<b>3.6520</b>
MF <sub>3</sub>	0.2416	<b>3.3269</b>	0.2912	<b>4.2523</b>
MF <sub>4</sub>	0.4534	4.4576	0.4583	4.3317
MF <sub>5</sub>	0.4799	3.7928	0.4800	3.7925
MF <sub>6</sub>	0.4976	3.6609	0.4976	3.6611
MF <sub>7</sub>	0.1851	2.9943	0.1851	2.9942
MF <sub>8</sub>	0.1411	2.5563	0.1411	2.5564
Processing Time (s)	5.72614 (s)		6.48926 (s)	

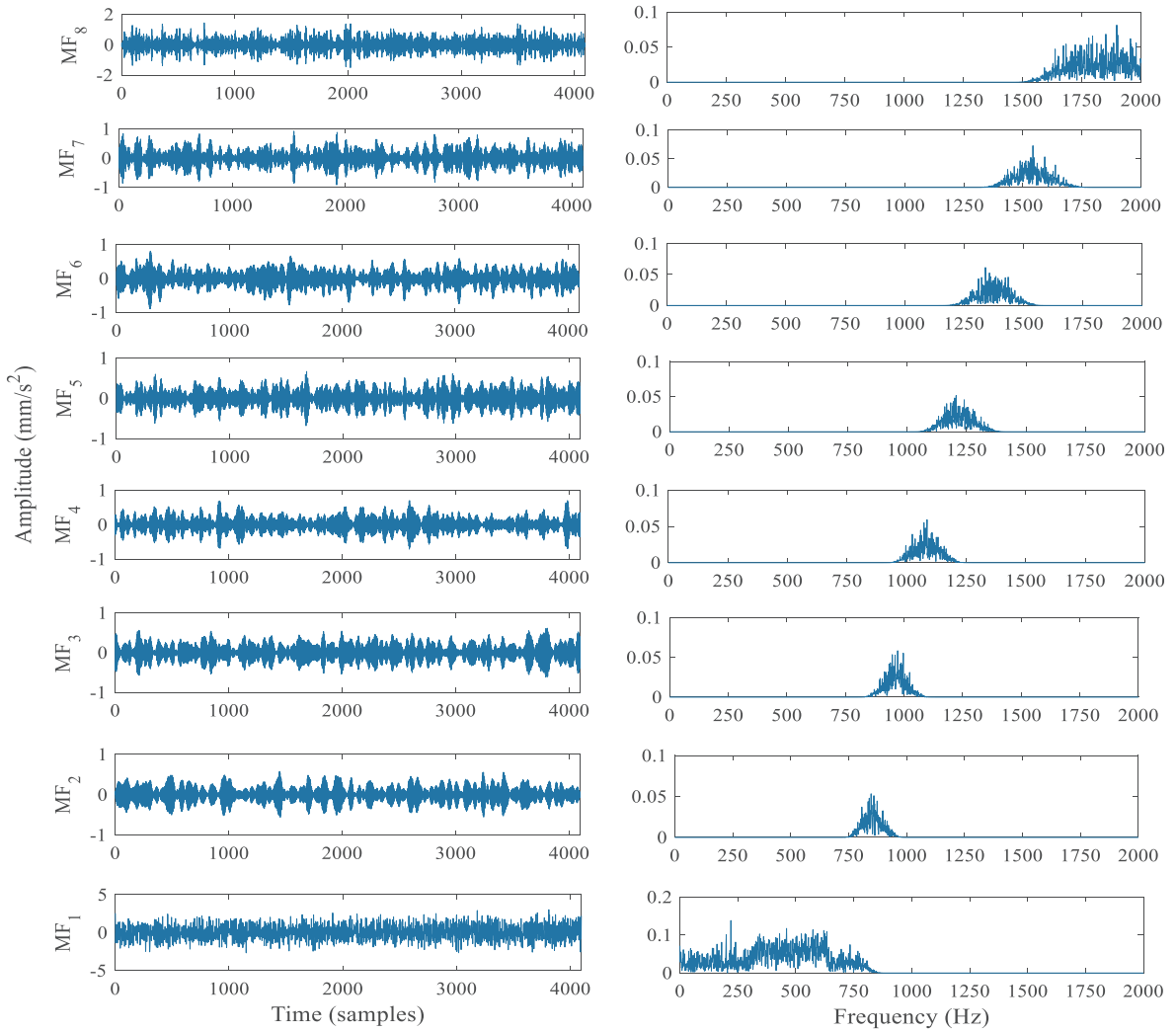


**Fig. 10.** Decomposition by FAWT into mode functions (MFs) and their FFTs.

through brake control module of NV Gate. A uniaxial accelerometer was mounted on the outer end of bearing case on the test gear shaft. Only one accelerometer was used and the vibrations were measured in the radial direction. Fig. 12(b) displayed below, shows the direction of the accelerometer to measure the vibrations.

**Table 4**  
Performance of CIs post FAWT.

Signal Decomposed mode	No fault Condition Indicator		With fault Condition Indicator	
	RMS	Kurtosis	RMS	Kurtosis
MF <sub>1</sub>	0.4332	3.0989	0.4295	2.9101
MF <sub>2</sub>	0.2345	3.1596	0.2502	3.0346
MF <sub>3</sub>	0.2236	3.1022	0.2263	2.8428
MF <sub>4</sub>	0.2057	2.7986	0.1972	2.9063
MF <sub>5</sub>	0.1997	2.9668	0.1972	3.1371
MF <sub>6</sub>	0.1950	3.0193	0.1862	2.8146
MF <sub>7</sub>	0.1720	2.7439	0.1860	3.5652
MF <sub>8</sub>	0.9693	2.5849	0.9608	2.5399
Processing Time (s)	8.3574		8.350	

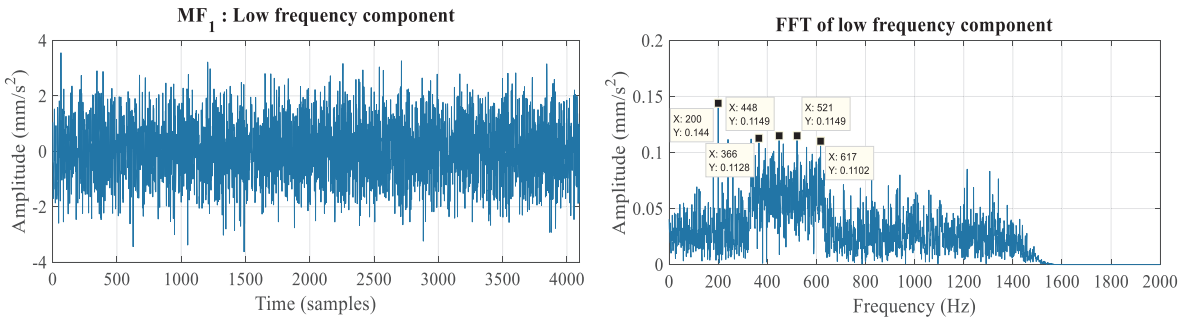


Fig. 11. Detail view of the decomposed mode functions and its FFT.

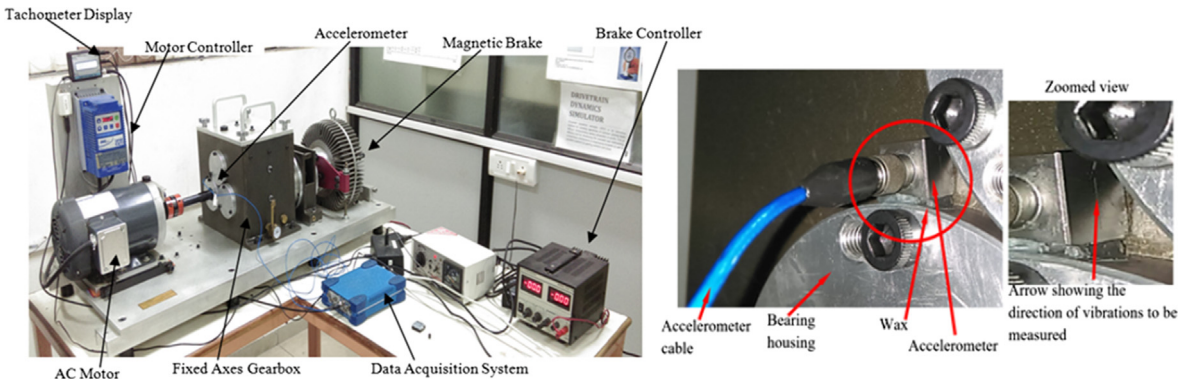


Fig. 12. Experimental setup, (a) test-rig, (b) accelerometer location.

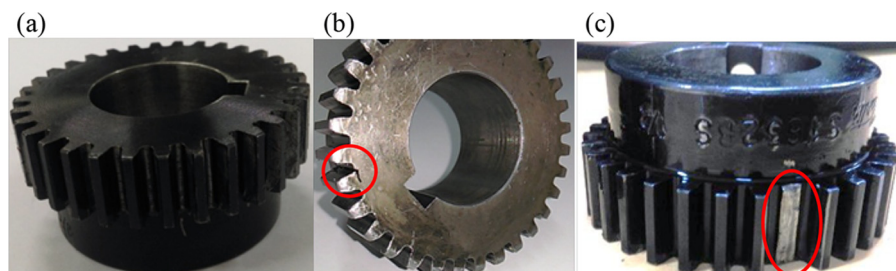


Fig. 13. Test gears, (a) Healthy gear, (b) cracked tooth gear, (c) missing tooth gear.

**Table 5**  
Gear specification.

Parameter	Input gear	Output gear
Number of teeth	32	80
Pressure Angle (°)	20	20
Diametral pitch (per mm)	0.6299	0.6299
Module (mm)	1.5879	1.5879
Face width	12.5	12.5

#### 4.2. Test gears

Involute spur gears of medium carbon steel (AISI1045) were used in this study. Different gear tooth faults i.e., gears with crack tooth and missing tooth as shown in Fig. 13 were used to examine the performance of VMD under real-time varying speed conditions. The details of the gears are listed in Table 5. The test gears were mounted on the main shaft. Faults like a crack in the tooth root of gears were introduced by wire EDM.

#### 4.3. Measurement conditions

The object of this study is to diagnose gear fault under real-time varying speed conditions. Based on literature review, signal acquisition for all the test gears were performed with a sampling rate of 12.5 kS/s at constant loading of 32Nm, which is 40% of the total load. The speed variation similar to Fig. 1 has been considered based on the history and operation of wind turbines [4,30] as shown in Fig. 14. Such varying speed profile has not yet studied before and incorporates all the non-linear fluctuations occurred during the run-up and coast-down.

#### 4.4. Demonstration of experimental results and performance evaluation

The vibration signals acquired experimentally for the aforementioned gear health under real-time varying speed conditions are shown in Fig. 15. From the experimentally recorded vibration signals, it was difficult to distinguish or specify the health of gear based on the appearance of vibration signals. However, few peaks were noticed occurring in both the crack tooth and missing tooth, which resemble transient peaks; however, the amplitude remains almost same of healthy gear and a missing tooth. The amplitude of the cracked tooth was observed less as compared to the amplitude of a healthy gear vibration signal. Further, when statistically analyzed the behavior of RMS and kurtosis as shown in Table 6 was again confusing. For example, fundamentally kurtosis of a healthy gear vibration signal is considered as 3 approximately, whereas in the present case, kurtosis value of healthy gear vibration signal was found 6.024 which contradicts the basic theory of kurtosis based statistical analysis. Further, for crack tooth gear and missing tooth gear, the values of kurtosis were noted as 12.33 and 5.80 respectively; however, these evaluated values conflict with the fact that kurtosis must increase with the increase in fault. Thus, fault symptoms were not clearly identified from raw vibration signals.

To investigate the performance of VMD, the raw vibration signals were decomposed by VMD and VMFs were extracted for different gear tooth health as shown in Fig. 16. The VMFs are plotted column-wise indicating healthy gear tooth, crack tooth gear and missing tooth gear. It was observed from the decomposed VMFs that the transients generated due to the meshing of the gears were clearly noticed as shown in Fig. 16. Further, with an increase in the fault level i.e. from healthy gear tooth to crack tooth gear to missing tooth gear the amplitude of the transient peaks was found increased relatively on comparing VMF<sub>2</sub>, VMF<sub>3</sub>, and VMF<sub>4</sub>. Further, it was also observed from the VMFs (VMF<sub>2</sub>, VMF<sub>3</sub>, and VMF<sub>4</sub>) that a regular pattern of transients was appearing when the speed increases. As clearly found from the simulation study that VMD is capable of separating the modes, therefore, the FFTs of the experimental signals are not plotted. Nevertheless, the decomposed VMFs were analyzed statistically using RMS and kurtosis, their

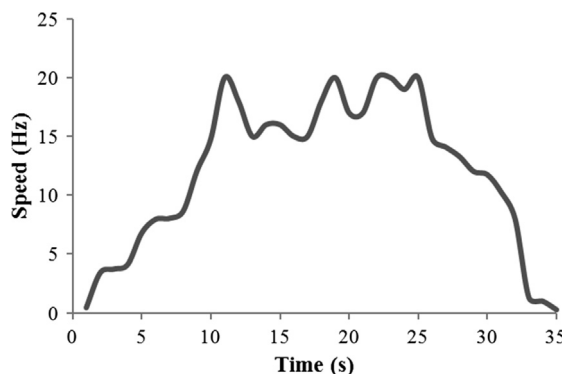


Fig. 14. Profile of real-time varying speed conditions.

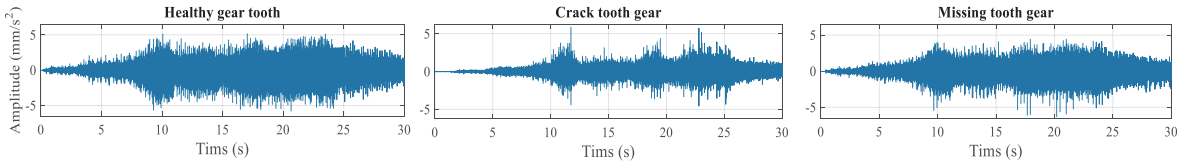


Fig. 15. Gear vibration signals correspond to different gear health.

**Table 6**  
Performance of CIs post VMD for experimental signals.

Method	Signal component	Healthy gear Condition Indicator		Crack tooth Condition Indicator		Missing tooth Condition Indicator	
		RMS	Kurtosis	RMS	Kurtosis	RMS	Kurtosis
	Raw vibration signal	0.8605	<b>6.0294</b>	1.5975	<b>12.3388</b>	0.7417	<b>5.8036</b>
VMD	VMF <sub>1</sub>	0.4608	<b>3.5880</b>	0.4424	<b>4.1937</b>	0.3862	<b>5.9110</b>
	VMF <sub>2</sub>	0.3295	<b>3.9832</b>	0.5828	<b>8.7684</b>	0.2552	<b>11.9155</b>
	VMF <sub>3</sub>	0.1620	<b>4.2942</b>	0.4941	<b>10.5502</b>	0.2718	<b>14.9585</b>
	VMF <sub>4</sub>	0.1325	5.1592	0.4495	7.3013	0.1268	12.0521
	VMF <sub>5</sub>	0.1174	4.2571	0.3663	9.0663	0.0744	9.6138
	Processing Time (s)	74.95		87.08		166.53	
EWT	MF <sub>1</sub>	0.0078	<b>4.0087</b>	0.0270	<b>4.9250</b>	0.0054	<b>5.2700</b>
	MF <sub>2</sub>	0.0082	3.3413	0.0820	3.2961	0.0912	3.3748
	MF <sub>3</sub>	0.1784	5.2504	0.0295	4.2651	0.1914	5.3140
	MF <sub>4</sub>	0.1281	5.6145	0.0411	4.2087	0.1219	6.5159
	MF <sub>5</sub>	0.1687	2.99063	0.1500	5.1637	0.1544	2.9540
	Processing Time (s)	4332.50		5112.39		6925.8	
FAWT	MF <sub>1</sub>	0.3590	5.4091	0.6607	5.4168	0.2822	5.7067
	MF <sub>2</sub>	0.1810	4.6241	0.3735	6.2926	0.1457	4.4031
	MF <sub>3</sub>	0.1796	4.2943	0.3355	5.9378	0.1673	4.2067
	MF <sub>4</sub>	0.2383	4.8457	0.3204	6.9294	0.2062	4.7243
	MF <sub>5</sub>	0.1956	4.4213	0.3139	6.3966	0.1790	4.2381
	Processing Time (s)	1511.19		1247.46		1277.21	

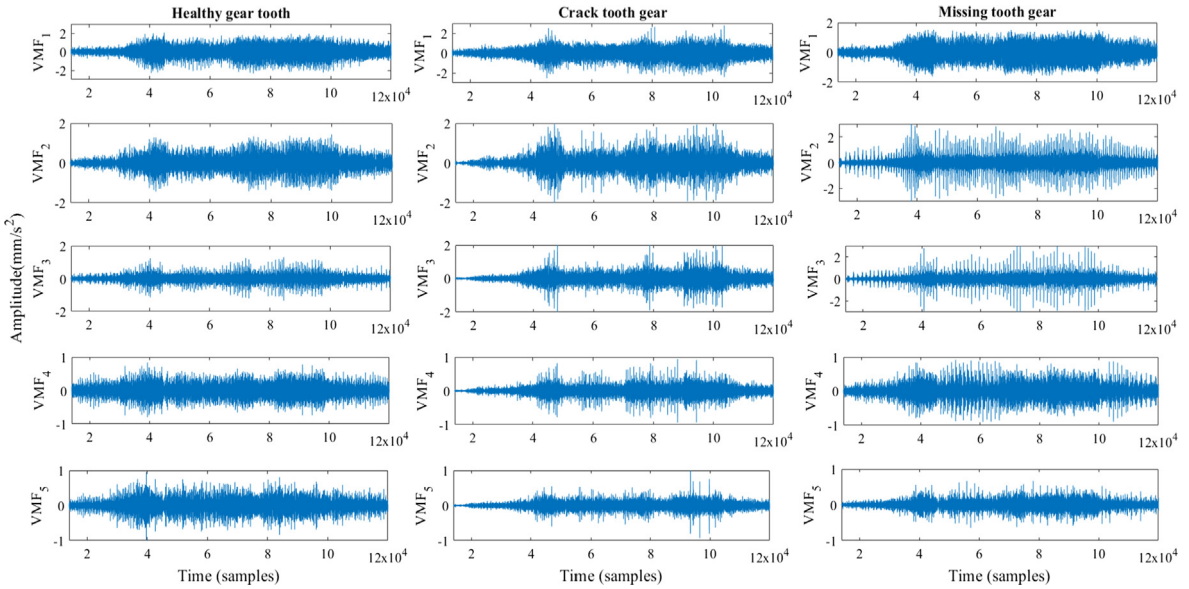
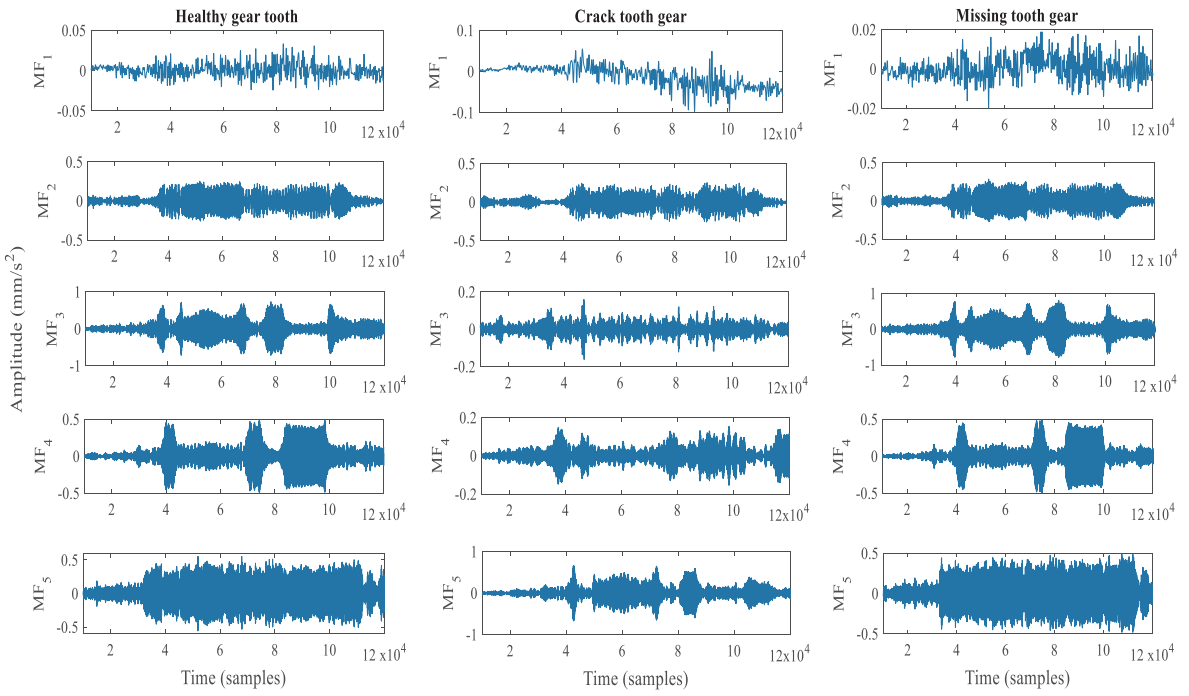


Fig. 16. Decomposed mode functions using VMD.

responses are reported in Table 6. The performance of kurtosis also favors the decomposition performed by VMD, i.e., kurtosis was found increased with increased fault levels for the decomposed VMFs. Further, the kurtosis value of the VMF<sub>1</sub> of healthy gear was found 3.58, which makes the fact valid that kurtosis of healthy gear is nearly 3. In a gear vibration signal, variance increases due to the presence of fault as well as the variation of the speed of gear rotation, therefore kurtosis increases because it is based on the



**Fig. 17.** Decomposed mode functions using EWT.

variance of the signal. VMD decomposed the signal by exposing the transient peaks significantly, thus variance is evaluated considering these transients, and consequently, kurtosis exhibited the increased trend for increased fault severity. Despite higher value than 3, the kurtosis value of other VMFs displayed increasing values for increasing faults. However, the indications of RMS toward crack tooth fault and missing tooth fault with respect to healthy gear tooth were confusing.

To contrast the performance of the VMD based decomposition, EWT was also used to test its decomposition capability. The decomposed MFs using EWT are displayed column-wise for healthy gear tooth, crack tooth gear and missing tooth gear in Fig. 17. It was observed from Fig. 17 that EWT decomposed the signals, however, the decomposed components did not display any indication towards the presence of embedded faulty transients. The amplitude of the decomposed MF<sub>1</sub> was decreased for faulty signal components relatively to healthy gear tooth signal components. However, the value of kurtosis was observed increased for increased fault severity as shown in Table 6. Further, the processing time for extracting the MFs using EWT was found very high as compared to VMD.

The performance of VMD was also compared to FAWT, the decomposed MFs using FAWT are shown in Fig. 18 and reports of kurtosis and RMS are presented in Table 6. From the decomposed MFs using FAWT, the occurrence of transients was observed very imprecise as compared to VMD. When compared the MFs decomposed by FAWT, the amplitude was found increased for crack tooth gear and decreased for missing tooth gear. Fundamentally, this cannot be valid because, when there is a missing tooth, there will be an impact in between the gear teeth and sudden amplitude gain must occur at that instant which will generate impulses in the time domain vibration signal, which were missing in the present case when decomposed by FAWT. Few transient impulses were observed in different decomposed MFs for crack tooth gear but when compared with equivalent VMF, these MFs were found least effecting in exhibiting transients.

Moreover, the time consumed for processing the raw vibration signals and to extract the MFs was also large as compared to the VMD. The statistical analysis condition indicators RMS and kurtosis were observed senseless as they did not respond to the increased fault severity. This also validates that FAWT is least capable of decomposing vibration signals under such real-time varying speed conditions. All these experimental investigation and analysis of the time domain signal was performed on the same computer as mentioned above.

An important point to highlight is that the optimum number of decomposed sub-bands is very important, i.e., if the signal is decomposed more, the vibration signal may lose the significant fault features used for fault extractions. Thus, further research is required for optimum decomposed sub-bands under varying speed conditions. Thus, the performance of the proposed method may vary upon the selection of the parameters used for the VMD evaluation.

## 5. Conclusion

This study analyses the performance of VMD based fault diagnosis approach by exhibiting the faulty transients under real-time varying speed conditions. The vibration signals of gearbox for different localized gear tooth faults under varying speed conditions

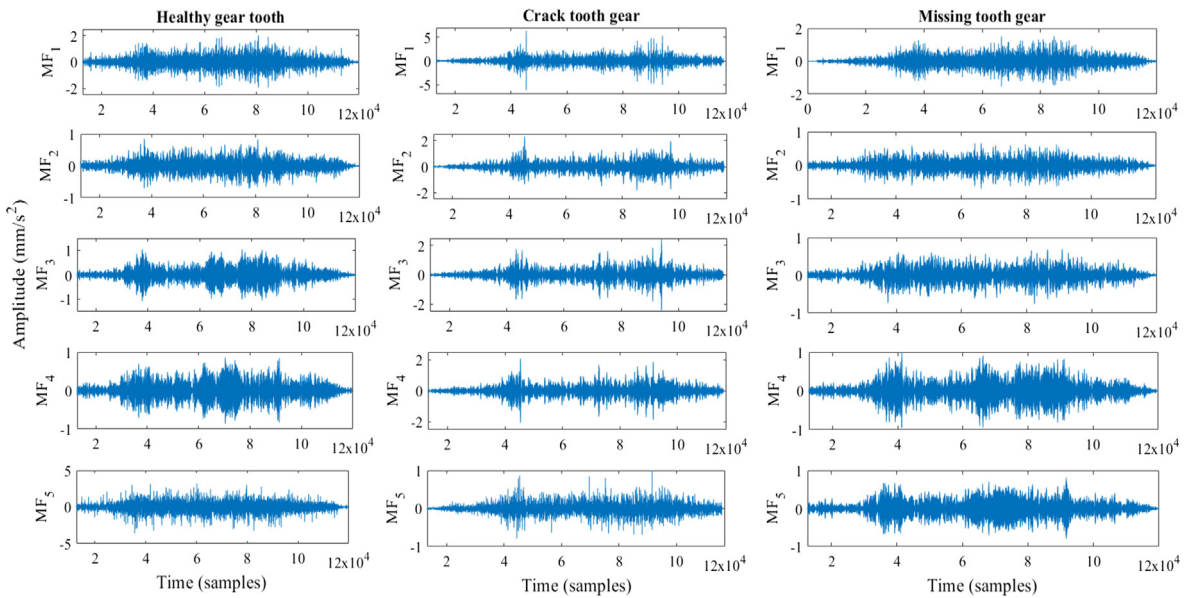


**Fig. 18.** Decomposed mode functions using FAWT.

were acquired and analyzed using signal-processing as well as statistically using RMS and kurtosis. To expose the fault transients, VMD was used for both simulated signals and experimental signals indicating the presence of faults. FFTs of VMD decomposed components were investigated to seek the presence of fault-related frequencies, which were clearly observed from the simulation study. It was also observed that kurtosis did sense the presence of fault transients in VMFs both for simulated and experimental signals. To state the effectiveness of the VMD, a comparison is performed along with the signals analyzed by both EWT and FAWT. Under varying speed and presence of faults in experimental signals, VMD displayed efficient separation of the different modes that correspond to the variation in speed and the effect of transient impulses due to a cracked tooth and a missing tooth. The fault detection performance of VMD was found better than EWT and negligible by FAWT for both simulated and experimental signals. Further EWT, need improvement in the effective decomposition of vibration signal recorded under such type of varying speed conditions.

#### Declaration of Competing Interest

The authors declared that there is no conflict of interest.

#### Appendix A. Supplementary material

Supplementary data to this article can be found online at <https://doi.org/10.1016/j.engfailanal.2019.104204>.

#### References

- [1] Z. Feng, M. Liang, Y. Zhang, S. Hou, Fault diagnosis for wind turbine planetary gearboxes via demodulation analysis based on ensemble empirical mode decomposition and energy separation, *Renew. Energy* 47 (2012) 112–126.
- [2] K. Wang, Y. Wang, D. Luo, Q. He, Application of order tracking rationale to non-rotating cantilever beam analysis, in: Prognostics and Health Management (PHM), 2014 IEEE Conference on, IEEE, 2014, June, pp. 1–6.
- [3] Y. Lei, D. Han, J. Lin, Z. He, Planetary gearbox fault diagnosis using an adaptive stochastic resonance method, *Mech. Syst. Sig. Process.* 38 (1) (2013) 113–124.
- [4] <http://www.sotaventogalicia.com/en/real-time-data/historical>.
- [5] Z. Feng, X. Chen, M. Liang, Iterative generalized synchrosqueezing transform for fault diagnosis of wind turbine planetary gearbox under non-stationary conditions, *Mech. Syst. Sig. Process.* 52 (2015) 360–375.
- [6] P.D. Samuel, D.J. Pines, A review of vibration-based techniques for helicopter transmission diagnostics, *J. Sound Vibrat.* 282 (2005) 475–508.
- [7] V. Sharma, A. Parey, Gear crack detection using modified TSA and proposed fault indicators for fluctuating speed conditions, *Measurement* 90 (2016) 560–575.
- [8] V. Sharma, A. Parey, Gearbox fault diagnosis using RMS based probability density function and entropy measures for fluctuating speed conditions, *Struct. Health Monit.* 16 (6) (2017) 682–695.
- [9] X. Liang, M.J. Zuo, Z. Feng, Dynamic modeling of gearbox faults: A review, *Mech. Syst. Sig. Process.* 98 (2018) 852–876.
- [10] V. Sharma, A. Parey, A review of gear fault diagnosis using various condition indicators, *Procedia Eng.* 144 (2016) 253–263.
- [11] M.S. Kan, A.C. Tan, J. Mathew, A review on prognostic techniques for non-stationary and non-linear rotating systems, *Mech. Syst. Sig. Process.* 62 (2015) 1–20.
- [12] Cohen, Leon, Time-frequency analysis, vol. 778, Prentice Hall, 1995.
- [13] N.E. Huang, Z. Shen, S.R. Long, M.C. Wu, H.H. Shih, Q. Zheng, H.H. Liu, The empirical mode decomposition and the Hilbert spectrum for nonlinear and non-stationary time series analysis, *Proc. Roy. Soc. London A: Math., Phys. Eng. Sci.* 454 (1971) (1998) 903–995.
- [14] K. Dragomiretskiy, D. Zosso, Variational mode decomposition, *IEEE Trans. Signal Process.* 62 (3) (2014) 531–544.
- [15] X. Chen, Z. Feng, Iterative generalized time-frequency reassignment for planetary gearbox fault diagnosis under non-stationary conditions, *Mech. Syst. Sig. Process.*

- Process. 80 (2016) 429–444.
- [16] B. Chen, Z. Zhang, C. Sun, B. Li, Y. Zi, Z. He, Fault feature extraction of gearbox by using overcomplete rational dilation discrete wavelet transform on signals measured from vibration sensors, *Mech. Syst. Sig. Process.* 33 (2012) 275–298.
- [17] C. Junsheng, Y. Dejie, Y. Yu, Research on the intrinsic mode function (IMF) criterion in EMD method, *Mech. Syst. Sig. Process.* 20 (4) (2006) 817–824.
- [18] X. An, H. Zeng, C. Li, Envelope demodulation based on variational mode decomposition for gear fault diagnosis, *Proc. Instit. Mech. Eng., Part E: J. Process Mech. Eng.* 231 (4) (2017) 864–870.
- [19] A. Parey, R.B. Pachori, Variable cosine windowing of intrinsic mode functions: Application to gear fault diagnosis, *Measurement* 45 (3) (2012) 415–426.
- [20] V. Sharma, A. Parey, Frequency domain averaging based experimental evaluation of gear fault without tachometer for fluctuating speed conditions, *Mech. Syst. Sig. Process.* 85 (2017) 278–295.
- [21] Y. Deng, W. Wang, C. Qian, Z. Wang, D. Dai, Boundary-processing-technique in EMD method and Hilbert transform, *Chin. Sci. Bull.* 46 (11) (2001) 954–960.
- [22] C. Zhong, Z. Shixiong, Analysis on end effects of EMD method, *J. Data Acquisition Process.* 1 (2003) 025.
- [23] T. Wang, M. Zhang, Q. Yu, H. Zhang, Comparing the applications of EMD and EEMD on time-frequency analysis of seismic signal, *J. Appl. Geophys.* 83 (2012) 29–34.
- [24] Q. Jiang, B.W. Suter, Instantaneous frequency estimation based on synchrosqueezing wavelet transform, *Signal Process.* 138 (2017) 167–181.
- [25] R.U. Maheswari, R. Umamaheswari, Application of Wavelet synchrosqueezing transform for wind turbine gearbox fault diagnosis, in: Computational Intelligence and Computing Research (ICCIC), 2016 IEEE International Conference on, IEEE, 2016, December, pp. 1–4.
- [26] J. Hu, J. Wang, L. Xiao, A hybrid approach based on the Gaussian process with t-observation model for short-term wind speed forecasts, *Renew. Energy* (2017) 670–685.
- [27] Y. Kong, T. Wang, F. Chu, Meshing frequency modulation assisted empirical wavelet transform for fault diagnosis of wind turbine planetary ring gear, *Renew. Energy* 132 (2019) 1373–1388.
- [28] F. Chaari, W. Bartelmus, R. Zimroz, T. Fakhfakh, M. Haddar, Gearbox vibration signal amplitude and frequency modulation, *Shock Vib.* 19 (4) (2012) 635–652.
- [29] Y.S. Kim, I.Y. Chung, S.I. Moon, An analysis of variable-speed wind turbine power-control methods with fluctuating wind speed, *Energies* 6 (7) (2013) 3323–3338.
- [30] <http://dromstørre.dk/wpcontent/wind/miller/windpower%20web/en/tour/wres/variab.htm>.
- [31] A.M.I. Ferdous, M.R.I. Sheikh, M.A. Shobug, Controlling of frequency fluctuation of wind turbine generator using wind speed controlled pitch controller, in: Electrical, Computer & Telecommunication Engineering (ICECTE), International Conference on, IEEE, 2016, December, pp. 1–4.
- [32] J.R. Connell, The spectrum of wind speed fluctuations encountered by a rotating blade of a wind energy conversion system, *Sol. Energy* 29 (5) (1982) 363–375.
- [33] R. Wagner, I. Antoniou, S.M. Pedersen, M.S. Courtney, H.E. Jørgensen, The influence of the wind speed profile on wind turbine performance measurements, *Wind Energy: Int. J. Progr. Appl. Wind Power Convers. Technol.* 12 (4) (2009) 348–362.
- [34] V. Sharma, A. Parey, Performance evaluation of decomposition methods to diagnose leakage in a reciprocating compressor under limited speed variation, *Mech. Syst. Sig. Process.* 125 (2019) 275–287.
- [35] A. Upadhyay, M. Sharma, R.B. Pachori, Determination of instantaneous fundamental frequency of speech signals using variational mode decomposition, *Comput. Electr. Eng.* 62 (2017) 630–647.
- [36] Y. Wang, R. Markert, J. Xiang, W. Zheng, Research on variational mode decomposition and its application in detecting rub-impact fault of the rotor system, *Mech. Syst. Sig. Process.* 60 (2015) 243–251.
- [37] İ. Bayram, An analytic wavelet transform with a flexible time-frequency covering, *IEEE Trans. Signal Process.* 61 (5) (2013) 1131–1142.
- [38] J. Gilles, Empirical wavelet transform, *IEEE Trans. Signal Process.* 61 (16) (2013) 3999–4010.
- [39] S. Sheng, Wind turbine gearbox condition monitoring round Robin study-vibration analysis (No. NREL/TP-5000-54530), National Renewable Energy Lab. (NREL), Golden, CO (United States), 2012.
- [40] H. Ma, X. Pang, R. Feng, R. Song, B. Wen, Fault features analysis of cracked gear considering the effects of the extended tooth contact, *Eng. Fail. Anal.* 48 (2015) 105–120.
- [41] M. Zhao, J. Lin, X. Wang, Y. Lei, J. Cao, A tacho-less order tracking technique for large speed variations, *Mech. Syst. Sig. Process.* 40 (1) (2013) 76–90.
- [42] G. Dalpiaz, A. Rivola, R. Rubini, Effectiveness and sensitivity of vibration processing techniques for local fault detection in gears, *Mech. Syst. Sig. Process.* 14 (3) (2000) 387–412.
- [43] R.B. Randall, A new method of modeling gear faults, *J. Mech. Des.* 104 (2) (1982) 259–267.